

Critical properties in single crystals of $\text{Pr}_{1-x}\text{Pb}_x\text{MnO}_3$

B. Padmanabhan^{a,*}, H. L. Bhat^a, Suja Elizabeth^a

^a*Department of Physics, Indian Institute of Science,
Bangalore 560012, India*

Sahana Röbber^{b,c,d}, U.K. Röbber^b, K.Dörr^b, K. H.Müller^b

^b*IFW Dresden, Postfach 270016, D-01171 Dresden, Germany*

^c*Institut für Festkörperphysik, Technische Universität Dresden, D-01062 Dresden, Germany and*

^d*Max-Planck-Institut für Chemische Physik fester Stoffe,*

Nöthnitzer Str. 40, D-01187 Dresden, Germany

(Dated: December 9, 2021)

The critical properties at the ferromagnetic - paramagnetic transition have been analysed from data of static magnetization measurements on single crystals of $\text{Pr}_{1-x}\text{Pb}_x\text{MnO}_3$, for $x = 0.23$ and $x = 0.30$. In $\text{Pr}_{1-x}\text{Pb}_x\text{MnO}_3$ the ferromagnetic ordering and the metal-insulator transition do not coincide in parts of the phase diagram. The crystal with $x = 0.23$ is a ferromagnetic insulator with Curie temperature $T_C = 173$ K, while the crystal with $x = 0.30$ has $T_C = 198$ K and remains metallic up to a metal-insulator transition temperature $T_{MI} = 235$ K. The dc magnetization measurements were carried out in the field range from 0 to 5 T for an interval in the critical temperature range $T_C \pm 10$ K corresponding to a reduced temperature interval $0.003 < \epsilon < 0.6$. The exponents β for spontaneous magnetization, γ for the initial susceptibility above T_C and δ for the critical magnetization isotherm at T_C were obtained by static scaling analysis from modified Arrott plots and by the Kouvel Fisher method for the insulating crystal with composition $x = 0.23$. The data are well described by critical exponents similar to those expected for the Heisenberg universality class relevant for conventional isotropic magnets. Systematic deviations from scaling in the data for the metallic crystal with composition $x = 0.30$ are demonstrated from effective critical exponents near the assumed ordering transition. The unconventional magnetic ordering in this system indicates the presence of frustrated magnetic couplings that suppresses magnetic ordering and lowers the transition temperature.

PACS numbers: 75.47.Gk, 64.60.Fr, 75.40.Cx, 71.27.+a

I. INTRODUCTION

The research in rare earth manganites started around fifty years ago. The simultaneous occurrence of ferromagnetism and metallicity in these compounds has been explained by Zener's double exchange (DE) mechanism.¹ According to this mechanism in mixed-valence manganites the hopping of e_g electron from Mn^{3+} to Mn^{4+} ion mediated by the intervening $2p$ level of the O^{2-} ion leads to a ferromagnetic alignment of the spins in the core-like t_{2g} states. In recent years there has been a revived interest in manganites because of the large colossal magnetoresistance (CMR) effect shown by these materials, which is caused by the suppression of spin scattering around the ferromagnetic transition temperature.^{2,3} The maximum CMR in manganites is shown by compositions which fall in the range $x = 0.30$ to $x = 0.45$.³ $\text{La}_{1-x}\text{Sr}_x\text{MnO}_3$ which is the canonical double exchange manganite with maximum metallicity and ferromagnetism has a paramagnetic-ferromagnetic (PM-FM)

ordering temperature up to about $T_C = 350$ K in this composition range. But it shows only relatively weak magnetoresistance.⁴ On the other hand, $\text{La}_{1-x}\text{Ca}_x\text{MnO}_3$ has a low $T_C \simeq 250$ K at optimal doping and shows a sharp metal-insulator (MI) transition at a similar temperature T_{MI} with an associated large magnetoresistivity close to these temperatures.^{5,6}

The PM-FM transition accompanied by the MI transition is seen as a crossover from localisation to delocalisation of charge carriers. Thus to elucidate the cause of CMR effect near the MI transition, one needs to understand the precise nature of the FM-PM transition. Due to the Jahn-Teller (JT) effect in the Mn^{3+} ions, one assumes that strong couplings exist between the itinerant e_g electron and JT phonons. This coupling to the lattice can result in the formation of polarons. Hence the MI transition can be described as a discontinuous transition between the mobile and localised polarons. As the mobile carriers are strongly coupled to the t_{2g} spins, this mechanism, extended by JT lattice couplings, can lead to the formation of spin-polarized polarons. This mechanism explains the link between an unconventional FM-PM transition and the MI transition by mobile spin polarons. Since this mechanism involves a discontinuous formation of polarons, Goodenough *et al.*⁷ suggested that the FM-

*corresponding author. fax: 91-80-360 2602, E-mail: paddu@physics.iisc.ernet.in

PM transition should be of first order. Contrary to this, most of the manganites show a second order phase transition at the Curie temperature T_C . The usual perception that the ferromagnetic transitions in the mixed-valence manganites are of second order is corroborated by the absence of hysteresis in the temperature variation of magnetization and the observation of a smaller entropy change from specific heat data across the transition. Theoretical investigations on the critical behavior of CMR manganites by Motome and Furukawa⁸ based on simplified DE models reveal that the FM–PM transition should belong to the Heisenberg universality class. The Heisenberg model assumes short-range interactions between localised spins. But, the range of exchange interactions in CMR manganites is not obvious due to the itinerant nature of the e_g electrons and the close link between metal like conductivity and ferromagnetism. Therefore, it is not clear whether the ferromagnetic manganites should generically behave like conventional isotropic magnets with a FM–PM transition belonging to the Heisenberg universality class.

From experiments, varied and in part contradictory results have been obtained using different measurement techniques and data analyses to determine the critical properties. In one of the earlier papers, Lofland *et al.*⁹ using microwave absorption technique on $\text{La}_{0.7}\text{Sr}_{0.3}\text{MnO}_3$, have estimated $\beta = 0.45$, which is close to the mean field exponent $\beta = 0.5$. However, Martin *et al.*¹⁰ report $\beta = 0.295$ for the same system from neutron scattering data, which is closer to the value of the exponent for the Ising model $\beta = 0.325$. In $\text{La}_{1-x}\text{Ca}_x\text{MnO}_3$, the nature of the transition is found to be extremely sensitive to the divalent doping concentration. For example, in composition $x = 0.2$ which is a ferromagnetic insulator, a continuous transition is observed.¹¹ In ferromagnetic metallic $\text{La}_{1-x}\text{Ca}_x\text{MnO}_3$ for $x = 0.33$ a first order phase transition is observed, while a tricritical behavior has been reported for $x = 0.4$.¹² The physical properties of Pb doped PrMnO_3 differ from those of the La-based manganites, since Pr^{3+} has a lower ionic radius than La. Hence the system has a reduced average radius of the A-site ions, $\langle r_A \rangle$, and a lower T_C . Interestingly, in a certain doping range, this manganite system shows a rather wide temperature interval with a paramagnetic metallic state above T_C and below the maximum in the resistivity curve $\rho(T)$ at T_{MI} that signals the metal-insulator transition.¹³ Hence, depending on the doping level, one finds in the phase diagram for $\text{Pr}_{1-x}\text{Pb}_x\text{MnO}_3$ a PM–FM transition from a metallic paramagnetic phase into a ferromagnetic phase. This feature is unusual because in the majority of the mixed-valent ferromagnetic manganites one finds $T_C \simeq T_{\text{MI}}$. Indeed, assuming that the DE mechanism is responsible for the ferromagnetic order, it is difficult to explain a wide intermediate paramagnetic phase with metal-like conductivity. At lower doping one finds a transition between an insulating paramagnetic phase into a ferromagnetic insulating phase. However in the vicinity of T_C a metal-like conductivity behavior is observed. In

a simple picture, the presence of a band of mobile carriers should mediate a sufficiently strong ferromagnetic exchange to drive a ferromagnetic ordering transition. On the other hand, the presence of PM–FM transitions in mixed-valent manganites without a metal-like conductivity is well-known and mechanisms to explain such phases have been proposed.¹⁴ Here, localization of carriers due to strong electron-lattice coupling via Jahn-Teller effects or disorder may prevent metallic conductivity, while the DE-exchange mechanism remains sufficiently strong to ensure a PM–FM transition. In view of the unusual phase diagram of the $\text{Pr}_{1-x}\text{Pb}_x\text{MnO}_3$ system, an investigation on the critical point phenomena at its PM–FM transition and a comparison between the insulating and the metallic ferromagnets from this system is of high interest to disentangle the mechanisms leading to ferromagnetic order and to MI transitions in the mixed-valent manganites.

II. METHODS

A. Experimental Details

Single crystals of $\text{Pr}_{1-x}\text{Pb}_x\text{MnO}_3$ were grown by the flux technique.¹⁵ The phase was confirmed by powder X-ray diffraction and compositions were determined by energy dispersive X-ray analysis (EDAX) and subsequently by inductively coupled plasma atomic emission spectroscopy (ICPAES) for higher precision. From the grown crystals, two compositions, $x = 0.23$ and $x = 0.30$ were selected for the present study. Basic physical properties of the crystals from this compound series have been determined earlier, as reported in Ref 13. The crystal with composition, $x = 0.23$ is a ferromagnetic insulator with a Curie temperature T_C of about 173 K, which was estimated from temperature variation of magnetization carried out at 0.01 T.¹³

The $x = 0.30$ composition has $T_C = 200$ K and it undergoes an MI transition at 235 K with a peak magnetoresistance value of 93% near T_{MI} .¹³ For the present studies dc magnetization measurements M vs. H were carried out in the temperature range 155 to 179 K for $x = 0.23$ and from 188 to 214.5 K for $x = 0.30$ in external fields up to 5 T. The magnetization measurements were carried out by using commercial SQUID magnetometer (Quantum Design). The magnetic field was applied along the long edge of the platelet shaped crystals to minimize demagnetization effects. The orientation of these crystals has been determined by X-ray diffraction. It shows that the magnetic field has been oriented within a few degrees along a $\langle 100 \rangle$ direction of the pseudocubic perovskite crystal structure of our crystals. The effective internal field H_{eff} used for the scaling analysis has been corrected for demagnetization, $H_{\text{eff}} = H_{\text{appl}} - DM$, where D is the demagnetization factor obtained from M vs. H measurements in the low-field linear response regime at 10 K. In addition, specific heat measurements through the PM–FM transition were carried out by a PPMS (Quantum

Design). The detailed analysis of specific heat studies on these crystals will be published elsewhere.

B. Scaling analysis

The critical properties of a magnetic system showing a second order phase transition are characterized by critical exponents α , β , γ and δ and the magnetic equation of state which connects the four exponents. The mathematical definitions of the exponents are given below: The specific heat near T_C is given by,

$$C_+(T) = A(\epsilon)^{-\alpha}/\alpha, \epsilon > 0 \quad (1)$$

$$C_-(T) = A'(\epsilon)^{-\alpha'}/\alpha', \epsilon < 0 \quad (2)$$

where A and A' are the critical amplitudes below and above T_C respectively, and $\epsilon = (T - T_C)/T_C$. Below T_C the temperature dependence of the spontaneous magnetization $M_S(T)$ is given by

$$M_S(T) = M_0(\epsilon)^{-\beta}; \epsilon < 0 \text{ for } H \rightarrow 0 \quad (3)$$

Above T_C , the initial susceptibility is given by,

$$\chi_0^{-1}(T) = (h_0/M_0)\epsilon^\gamma, \epsilon > 0 \quad (4)$$

At T_C , M and H are related as,

$$M = DH^{1/\delta}, \epsilon = 0 \quad (5)$$

Here M_0 , h_0/M_0 and D are the critical amplitudes.

In the critical region, the magnetic equation of state is given by

$$M(H, \epsilon) = \epsilon^\beta f_\pm(H/\epsilon^{\beta+\gamma}) \quad (6)$$

where f_+ for $T > T_C$ and f_- for $T < T_C$ are regular analytic functions. Equation (6) implies that M/ϵ^β as a function of $H/\epsilon^{\beta+\gamma}$ yields two universal curves, one for temperatures below T_C and the other for temperatures above T_C .

If a magnetic system is governed by various competing couplings and/or randomness, the properties in the critical region may show various systematic trends or crossover phenomena. In that case, it is useful to generalize the power-laws for the critical behavior by defining effective exponents through

$$\beta_{\text{eff}} = \frac{d(\ln M(\epsilon))}{d(\ln \epsilon)}, \quad \gamma_{\text{eff}} = -\frac{d(\ln \chi(\epsilon))}{d(\ln \epsilon)} \quad (7)$$

which depend on the separation ϵ from the critical point.^{16,17,18}

In the asymptotic limit $\epsilon \rightarrow 0$, the effective exponents approach the universal critical (asymptotic) exponent. The calculations of the logarithmic derivatives involves

large uncertainties. Therefore, we have used two different methods to obtain estimates on effective exponents: (i) The complete set of data $\ln M(\epsilon)$ or $\ln \chi(\epsilon)$ vs $\ln \epsilon$ is fitted through a 4th or 5th order polynomial. The derivatives are calculated analytically which gives a rough overview on the dependence of the effective exponents on ϵ . (ii) Further estimates on the effective exponents were derived from a method via parabolic fits, as proposed in Ref. [19], which is used here for different values of $k = 7 \dots 12$ neighbouring points.

III. RESULTS

Figs. 1(a) and (b) show the M vs. H plots for $x = 0.23$ and 0.3 , respectively, in the temperature range $T_C \pm 10$ K. Corresponding specific heat data are shown in the insets of Figs. 1(a) and 1(b). The magnetic transitions are marked by cusps in the specific heat data near T_C . This indicates that the transitions are likely to be of second order, i.e. continuous with a negative critical exponent $\alpha < 0$.

Figs. 2(a) and 2(b) show modified Arrott plots for $M^{1/\beta}$ vs. $(H_{\text{eff}}/M)^{1/\gamma}$ constructed from the M vs. H plots at the different temperatures by using trial critical exponents β and γ similar to those of the 3D Heisenberg magnets. For the data of $x = 0.23$ crystal, this choice produces a range of nearly parallel linear isothermal curves for higher fields. This indicates that the critical properties are close to those of isotropic 3D ferromagnets. For the $x = 0.30$ crystal, the modified Arrott plots display systematic nonlinearities. Other choices of trial exponents result in stronger deviations from linearity in the modified Arrott plots for both crystals. This has been checked for the values of mean-field, tricritical mean-field and 3D Ising-like exponents as trial exponents. Following a standard procedure, the modified Arrott plots were extrapolated to the y axis intercept corresponding to $M_S(T, 0)$. At T_C this extrapolated line passes through the origin. The inverse initial susceptibility $\chi^{-1}(T)$ is obtained from the ratio of the y intercept and the slope above T_C . The T_C for $x = 0.23$ lies between 167 K and 167.5 K, while that for $x = 0.30$ lies between 197.5 K and 198 K. For this extrapolation, we have used the values above a field of about 0.1 T for crystal with $x = 0.23$. For the crystal with $x = 0.3$ roughly linear portions of the modified Arrott plot towards high fields have been used, with more low field values closer to the assumed T_C . It is clear, that this approach is a compromise which averages out an important physical contributions to the critical behaviour in that case. The universal scaling laws are almost obeyed with the trial values of β and γ close to those of the 3D Heisenberg universality class for $x = 0.30$.

Plots of $M_S(T, 0)$ vs. T for both compositions are shown in Figs. 3(a) and 3(b). The values of T_C and β were obtained by fitting $M_S(T, 0)$ vs. T to Eq. (2). The $\chi^{-1}(T)$ vs. T plots are also shown in Figs. 3(a) and 3(b).

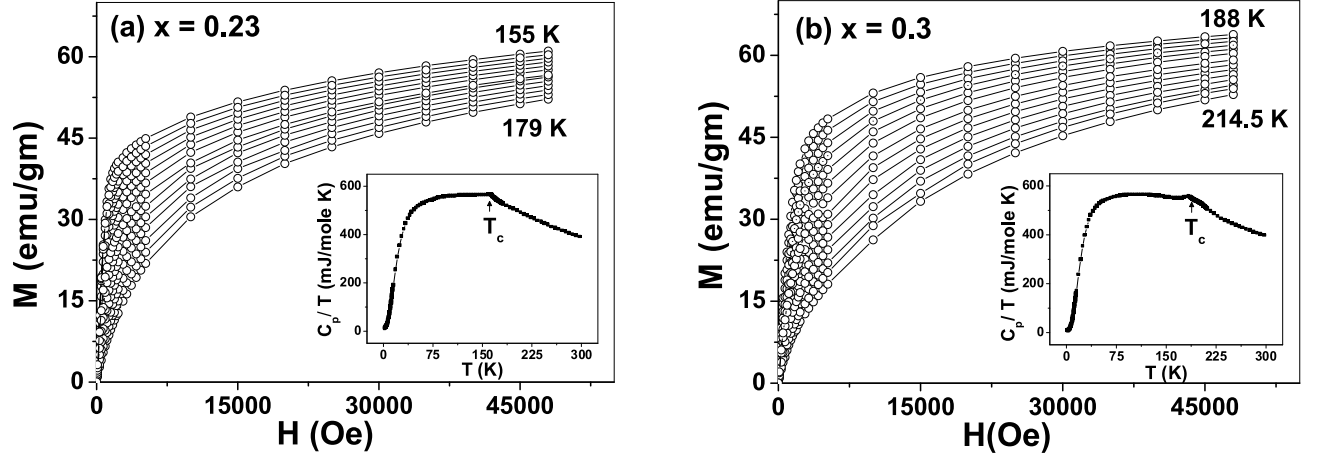


FIG. 1: Magnetization vs. field of $\text{Pr}_{1-x}\text{Pb}_x\text{MnO}_3$ for (a) $x = 0.23$ and (b) $x = 0.30$ from 0 to 5 T around T_C . Insets show the specific heat as C_p/T vs. T . Weak cusps are discernible at T_C indicating a second order transition.

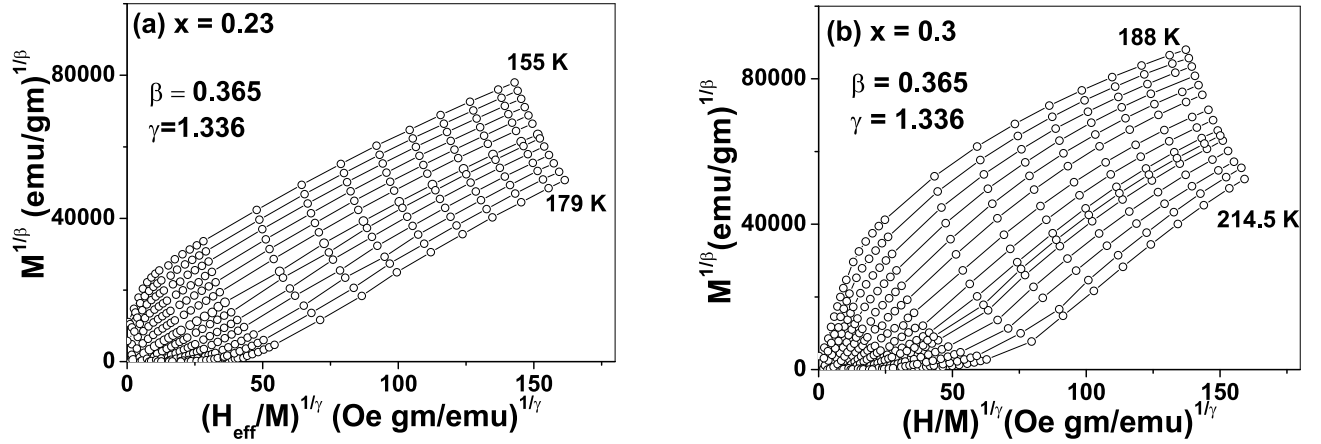


FIG. 2: Modified Arrott plots of $\text{Pr}_{1-x}\text{Pb}_x\text{MnO}_3$ for (a) $x = 0.23$ and (b) $x = 0.30$, where $\beta = 0.365$ and $\gamma = 1.336$ are the trial values corresponding to 3D Heisenberg ferromagnet.

We obtain γ and T_C by fitting $\chi^{-1}(T)$ to Eq. (4). This procedure is iterated by using the derived critical exponents again in a modified Arrott plot. Thus, a check has been made that the derived critical exponents are close to the trial exponents, and that the two critical temperatures T_C from the fits are the same within error estimates.

The exponents were also obtained by the Kouvel Fisher method,¹⁶ as shown in Figs. 4(a) and (b) where $M_S(T, 0)(dM_S(T, 0)/dT)^{-1}$ is plotted against T . The plots are straight lines with slope $1/\beta$ and T_C is the ratio of y intercept and slope. Similarly, in Figs. 4(a) and (b) we plot $\chi^{-1}(T)(d\chi^{-1}(T)/dT)^{-1}$ which shows a linear dependence. We have listed the critical exponents obtained from the modified Arrott plots as well as the Kouvel Fisher method along with T_C in Table 1. In Figs. 5(a) and (b), the critical isotherms M vs. H for both crystals are plotted, at 167 K and 197.5 K for $x = 0.23$ and 0.30 respectively. At the critical temperature M and H are related by Eq. (5). The high field region of the plot is a

straight line with slope $1/\delta$. The value of δ obtained for both compositions are given in Table 1. The three exponents derived from our static scaling analysis are related by the Widom scaling relation,

$$\delta = 1 + \gamma/\beta. \quad (8)$$

Using this scaling relation and the estimated values of β and γ we obtain δ values which are very close to the estimates for δ from the critical isotherms at T_C . Thus, the estimates of the critical exponents are consistent. In the critical region, the magnetization and applied field should obey the universal scaling behavior. In Figs. 6(a) and (b) we show plots of $M|\epsilon|^{-\beta}$ vs. $H|\epsilon|^{-(\beta+\gamma)}$ for $x = 0.23$ and 0.30 respectively. The two curves represent temperatures below and above T_C . The insets show the same data in log-log scale.

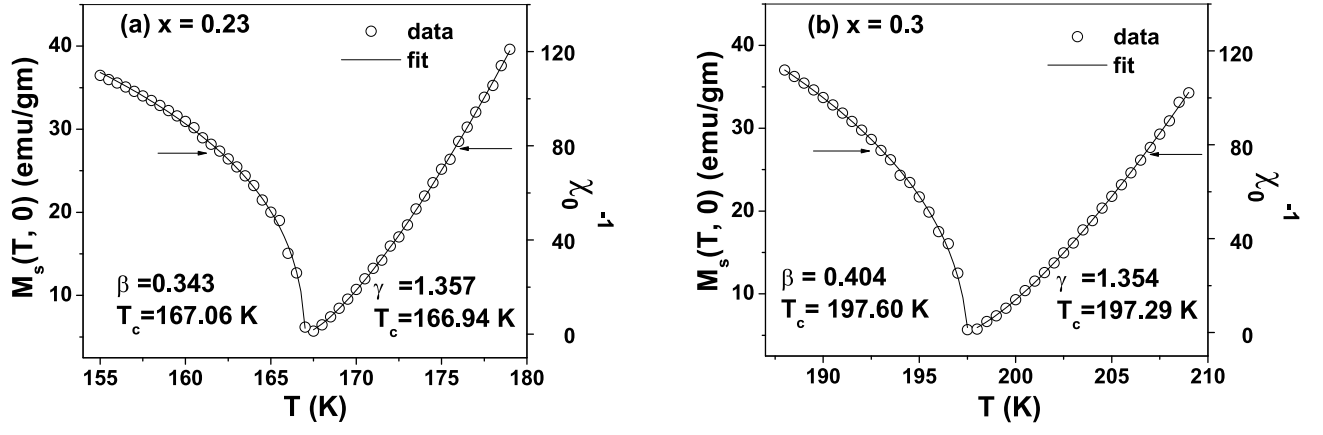


FIG. 3: Spontaneous magnetization (left) and initial susceptibility (right) vs. temperature of $\text{Pr}_{1-x}\text{Pb}_x\text{MnO}_3$ for (a) $x = 0.23$ and (b) $x = 0.30$ to determine β and γ respectively. (For clarity, only part of the $M(H)$ data measured around T_C are shown in this and next figure.)

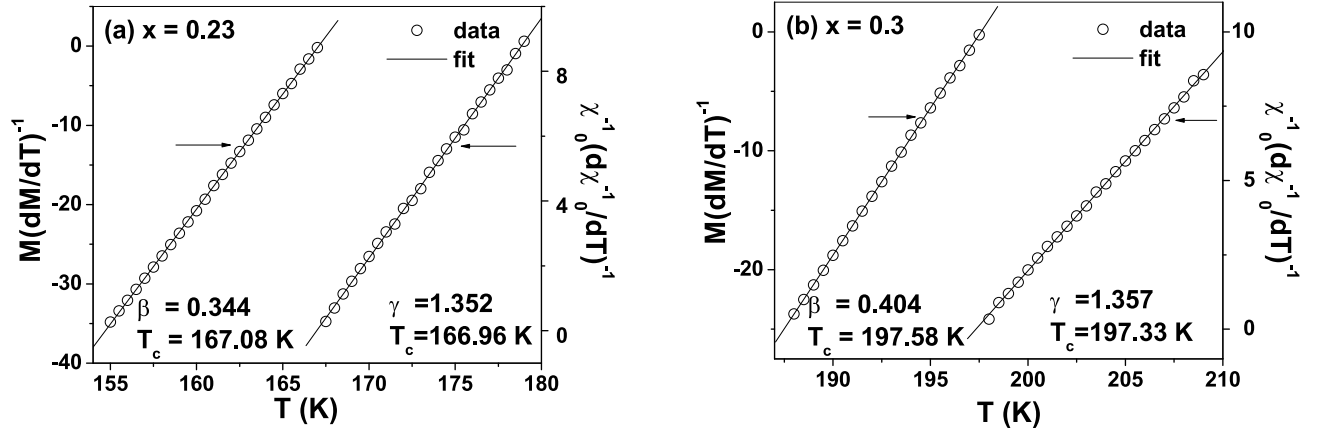


FIG. 4: Kouvel Fisher plots of $M_S(T, 0)(dM_S(T, 0)/dT)^{-1}$ and $\chi^{-1}(T)(d\chi^{-1}(T)/dT)^{-1}$ vs. T for determination of β and γ in $\text{Pr}_{1-x}\text{Pb}_x\text{MnO}_3$ for (a) $x = 0.23$ and (b) $x = 0.30$ respectively

IV. DISCUSSION

From our analysis, we see that the scaling is well obeyed for $x = 0.23$. The value of critical exponents of $\text{Pr}_{0.77}\text{Pb}_{0.23}\text{MnO}_3$ are consistent with those of the 3D Heisenberg ferromagnet that has critical indices $\beta_H = 0.368$, $\gamma_H = 1.396$, and $\delta_H = 4.80$.²⁰ This behavior is quite similar to other CMR manganites belonging to the universality class of 3D isotropic ferromagnets with short-range exchange couplings.^{21,22} The $x = 0.23$ composition is a ferromagnetic insulator at low temperatures. However this composition is on the crossover region of a MI-transition. Around T_C , there exists a small temperature range where it exhibits a metallic behavior as mentioned earlier.¹³ On the other hand, the scaling is poor for the crystal with composition $x = 0.3$, in particular towards low fields. The non-linearity in the modified Arrott plot indicate a non-conventional magnetic ordering behavior in this crystal. As remarked above, this crystal undergoes a metal insulator transition at 235 K. This temperature is about 35 K above the Curie temperature T_C , which is

quite unusual for conventional manganites.^{13,23} One way to interpret the data can be based on the observation that there are systematic deviations from Curie Weiss behavior below 250 K in this compound.¹³ This may indicate the formation of ferromagnetic clusters,²³ which results in a percolation mechanism for conduction and metallic behavior without a magnetic long-range order above T_C . Then, the non linearity of modified Arrott plots in Fig. 3(b) may be attributed to the presence of ferromagnetic clusters. However, the overall scaling behavior still indicates that some form of long-range magnetic order is finally established at the critical temperature T_C . In this case, the clustering behavior could be understood as a Griffiths phase with randomly varying local ordering temperature,²⁴ as proposed and described for ferromagnetic manganites in Refs. [25] and [26]. Clustering in the relevant models with random-temperature disorder for a Heisenberg-like magnet would yield complicated cross-over phenomena near criticality.¹⁷ In particular, from recent theoretical analysis for magnetic systems with correlated quenched-disorder, critical proper-

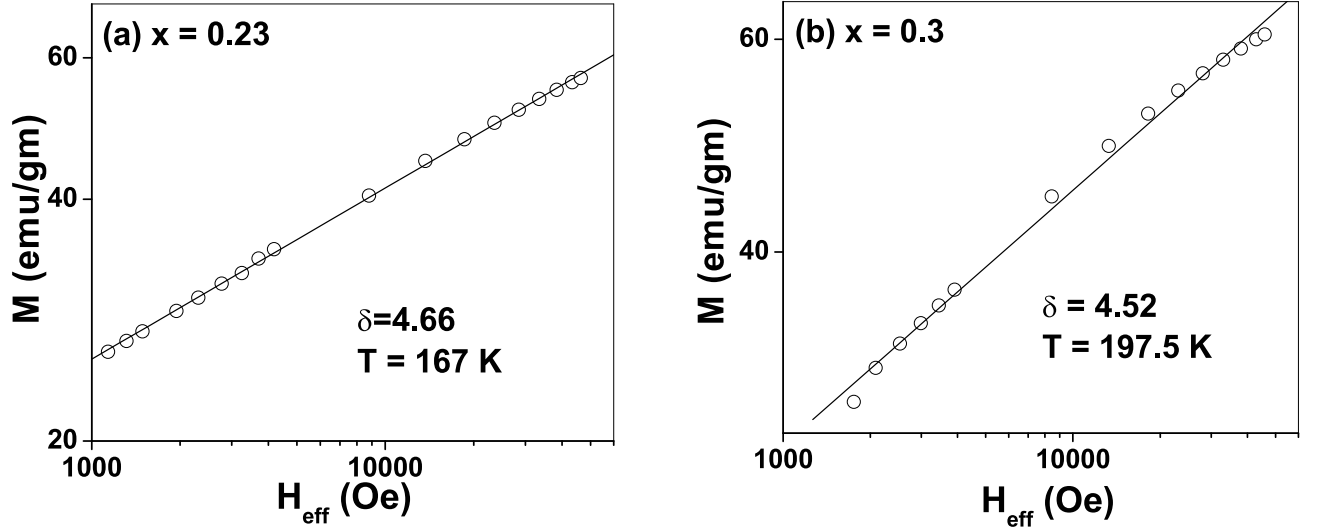


FIG. 5: Critical isotherms for $\text{Pr}_{1-x}\text{Pb}_x\text{MnO}_3$ for (a) $x = 0.23$ and (b) $x = 0.30$ corresponding to $T_C = 167 \text{ K}$ and $T_C = 200 \text{ K}$, respectively.

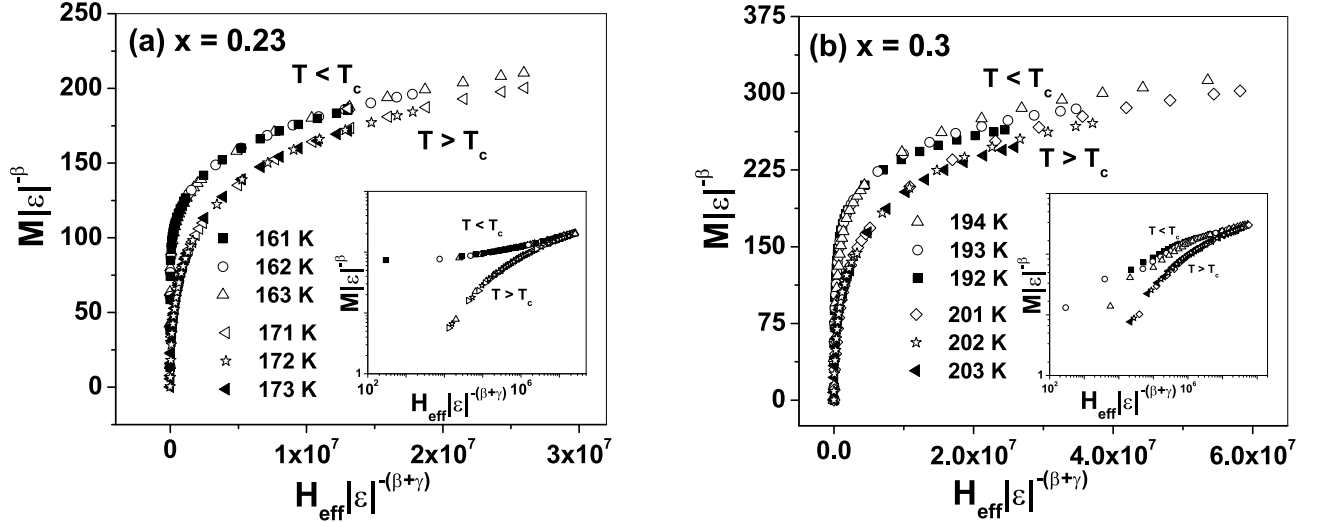


FIG. 6: Scaling plots for $\text{Pr}_{1-x}\text{Pb}_x\text{MnO}_3$ for (a) $x = 0.23$ and (b) $x = 0.30$ indicating two universal curves below and above T_C . The insets show the plots on a log - log scale.

ties with non-universal exponents have been found. For instance long-range correlated quenched-disorder, as described by the Weinrib-Halperin model with correlated random-temperature defects falling off as a power law r^{-a} with distance, can become relevant for Heisenberg-like magnets.²⁷ In the case of a 3D isotropic Heisenberg-like magnets, the critical exponents in this random-temperature model continuously vary with the exponent $a < 3$. From a field-theoretical calculation, values for β in the range 0.387 to 0.384 and remarkably increasing values of γ in the range 1.37 to 1.57 have been found.²⁸ On the other hand, Heisenberg-like systems may show values $\gamma > 1.41$ in the presence of extended impurities with dimensionality $\epsilon_d \geq 0.4$.²⁹ Otherwise, for non-correlated quenched disordered systems conventional Heisenberg-

like critical properties should be expected. Such conventional critical properties have been found for the rounded PM-FM transition in $\text{La}_{0.67}\text{Ca}_{0.33}\text{MnO}_3$ with low Ga-substitution on Mn-sites.³⁰ The results on that site diluted manganite with full control of the quenched disorder demonstrate that the ferromagnetic manganites do not generically own correlated random-temperature defects, that could lead to unconventional critical properties.

If there are correlated random-temperature defects in the present $\text{Pr}_{0.70}\text{Pb}_{0.30}\text{MnO}_3$ crystal, their influence must be weak. Otherwise, the static scaling should hold with a consistent, but non-universal set of critical exponents, in particular with an increased value of γ . As demonstrated by the extrapolation in the modified Ar-

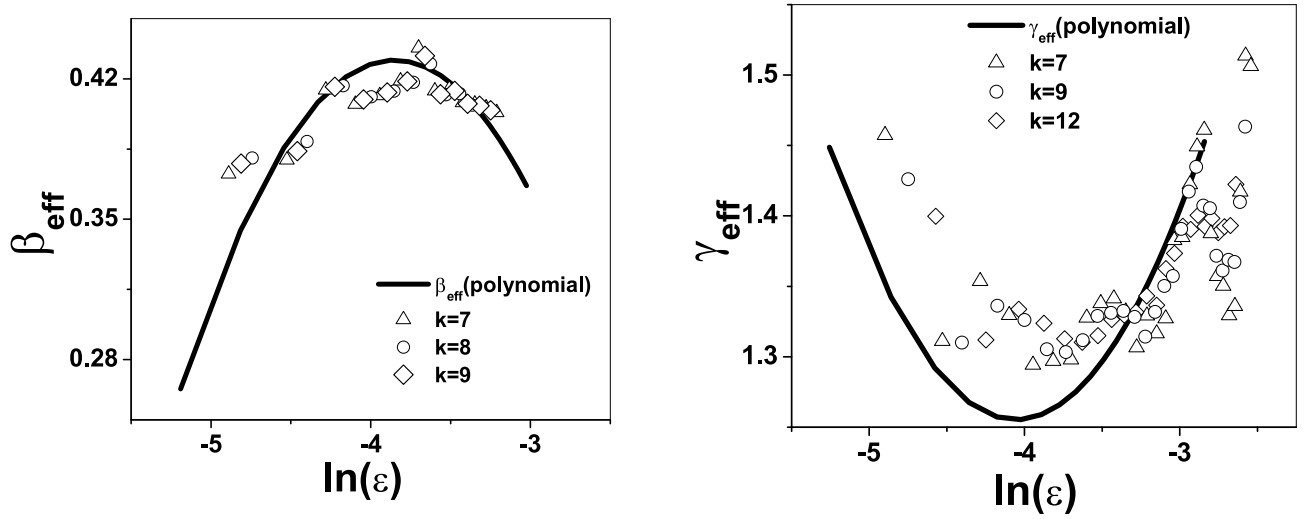


FIG. 7: Effective exponents (a) for static spontaneous magnetization β_{eff} below T_C and (b) for initial susceptibility above T_C vs. reduced temperature $\ln(\epsilon)$ for $\text{Pr}_{0.70}\text{Pb}_{0.30}\text{MnO}_3$. Logarithmic derivatives Eq. (7) are from polynomial fits (continuous thick line) and from a numeric error-improved method (Ref. [19]) using k neighbouring data points (symbols).

TABLE I: Evaluation of critical exponents of $\text{Pr}_{1-x}\text{Pb}_x\text{MnO}_3$.

Composition	Modified Arrott plots			Kouvel Fisher method			Critical isotherm	
	β	γ	$T_C(\text{average})$	β	γ	$T_C(\text{average})$	$\delta(\text{exp})$	$\delta(\text{calc})$ Eq. (8)
$x = 0.23$	0.343 ± 0.005	1.357 ± 0.020	167.00 ± 0.13	0.344 ± 0.001	1.352 ± 0.006	167.02 ± 0.04	4.69 ± 0.02	4.93
$x = 0.30$	0.404 ± 0.006	1.354 ± 0.020	197.46 ± 0.13	0.404 ± 0.001	1.357 ± 0.006	197.45 ± 0.04	4.73 ± 0.09	4.37

roth plot for relatively large fields and the scaling plot Fig. 6(b), we see an effective critical behavior in the crystal $x = 0.3$, that is roughly consistent with the properties of a Heisenberg-like magnet. Therefore, a clustering leading to a remarkable Griffiths phase effect seems insufficient to explain the anomalous magnetic ordering in our system.

The rounding effect, as seen in the modified Arrott plot Fig. 2(b), is pronounced close to the transition. As has been pointed out by Rivadulla et al.³¹ this behavior is often seen in various nominally ferromagnetic manganites. It indicates a suppression of ferromagnetic order by some further coupling effects that are effective on longer ranges and may lead to frustration. In fact, the modified Arrott plots resemble those proposed from theoretical considerations on magnets with frustrated couplings of random-field or random-anisotropy type,³² as found, e.g., in experiments on rare-earth based disordered magnets.³³ The presence of quenched random-fields is difficult to motivate for an overall ferromagnetic system in zero external fields, without very particular mechanisms. Hence, we should expect that the manganites behave as random anisotropy Heisenberg-like magnets. Quenched-random

anisotropies destroy the long-range magnetic order in isotropic magnets. But, long-range order could be re-established by anisotropic distributions of random axes and/or by weaker global cubic or uniaxial anisotropies.¹⁸

To discern the influence of such random magnetic couplings, we have plotted effective critical exponents for the crystal with composition $x = 0.3$ in Figs. 7(a) and (b). These effective exponents have been derived by the logarithmic derivatives Eq. (7) for the extrapolated $M_S(T, 0)$ and $\chi_0(T)$ from the modified Arrott plot. As usual, the estimates for γ_{eff} and β_{eff} are prone to large uncertainty reflected in the large scatter between the different numerical methods used for Fig. 7. However, there clearly is a systematic non-monotonous shift of the exponents with decreasing reduced temperature ϵ . In particular, γ_{eff} increases with increasing ϵ . A maximum or increasing γ_{eff} with larger ϵ has similarly been found in a recent investigation on a frustrated metallic ferromagnet.³⁴ Such systematic dependencies of γ_{eff} are suggested by theoretical investigations on effective critical properties of random anisotropy magnets.¹⁸ From our data, we cannot determine whether a plateau is reached for the effective exponents at small separation ϵ . It would correspond

to the values of the asymptotic exponents, if the transition is continuous. The data may also indicate a diverging γ_{eff} and vanishing β_{eff} . Such a behavior could indicate an infinite susceptibility phase or a quasi long-range ordered domain-like state, without macroscopic spontaneous magnetization as proposed for random-anisotropy systems.³² Thus the systematic shift of effective exponents suggest the presence of random symmetry breaking couplings in the magnetic system of the crystal with $x = 0.30$. Recent investigations on the Griffiths-like properties in paramagnetic $\text{La}_{1-x}\text{Sr}_x\text{MnO}_3$ also indicate that frustrated magnetic couplings may be present in the ferromagnetic manganites.²⁶ Such additional frustrating couplings explain for the $\text{Pr}_{0.70}\text{Pb}_{0.30}\text{MnO}_3$ crystal (i) the suppression of the magnetic transition temperature T_C below the MI transition temperature and the occurrence of a metal-like conductivity in a paramagnetic state (ii) the anomalous rounding as seen in the modified Arrott plot, and (iii) the markedly non-monotonous dependence of the effective critical exponents near the apparent magnetic ordering transition.

V. CONCLUSIONS

The static scaling analysis near the magnetic ordering on single crystals of $\text{Pr}_{1-x}\text{Pb}_x\text{MnO}_3$ for $x = 0.23$ and $x = 0.30$ has been performed to derive the critical exponents β , γ , and δ . These exponents were determined by extrapolating from relatively large fields. This means that we probe the system away from criticality at shorter lengths,

where the exchange mechanism is dominant. The critical exponents indicate that the underlying magnetic system in both the insulating and the metallic crystal is similar to that of a conventional isotropic magnet, as is expected for the manganites. The exponents are also consistent, as the Widom scaling relation between the exponents is obeyed. For the insulating crystal with composition $x = 0.23$ the data fit well with the universal scaling behavior. Thus, the magnetic properties in these crystals are those of an isotropic magnet with short-range exchange couplings. They are not subject to remarkable further effects as long-range magnetic couplings, that would lead to non-universal or mean-field properties. However, we can discern important magnetic coupling effects, which destroy proper universal scaling for the metallic crystal with $x = 0.30$. The scaling analysis as a conventional ferromagnet yields exponents, which average out the systematic drift seen in the effective exponents. Hence, there is evidence for an important cross-over effect in this crystal, which intercepts the formation of the conventional magnetic long-range order by frustrated magnetic couplings.

Acknowledgments

One of the authors(H.L.B.) acknowledges C.S.I.R (India) for financial support.

VI. REFERENCES

-
- ¹ C. Zener, Phys. Rev. **82**, 403 (1951).
 - ² *Colossal Magnetoresistive Oxides*, eds. Y. Tokura (Gordon & Breach Science Publishers, New York, 2000).
 - ³ *Colossal Magnetoresistance, Charge Ordering and relative properties of Magnetic oxides*, eds. C.N.R.Rao and B.Raveau (World Scientific Singapore, 1998).
 - ⁴ A. Urushibara, Y. Moritomo, T. Arima, A. Asamitsu, G. Kido, and Y. Tokura, Phys. Rev. B **51**, 14103 (1995).
 - ⁵ P. Schiffer, A.P. Ramirez, W. Bao, and S.-W. Cheong, Phys. Rev. Lett. **75**, 3336 (1995).
 - ⁶ C. Martin, A. Maignan, M. Hervieu, and B. Raveau, Phys. Rev. B **60**, 12191 (1999).
 - ⁷ W. Archibald, J. S. Zhou, and J. B. Goodenough, Phys. Rev. B **53**, 14445 (1996).
 - ⁸ Y. Motome and N. Furukawa, J. Phys. Soc. Jpn. **70**, 1487 (2001).
 - ⁹ S. E. Lofland, V. Ray, P. H. Kim, S. M. Bhagat, M. A. Manheimer, and S. D. Tyagi, Phys. Rev. B **55**, 2749 (1997).
 - ¹⁰ M. C. Martin, G. Shirane, Y. Endoh, K. Hirota, Y. Moritomo, and Y. Tokura, Phys. Rev. B **53**, 14285 (1996).
 - ¹¹ C. S. Hong, W. S. Kim, and N. H. Hur, Phys. Rev. B **63**, 92504 (2001).
 - ¹² D. Kim, B. Revaz, B. L. Zink, F. Hellman, J. J. Rhyne, and J. F. Mitchell, Phys. Rev. Lett. **89**, 227202 (2002).
 - ¹³ B. Padmanabhan, Suja Elizabeth, H. L. Bhat, Sahana Rössler, K. Dörr, and K. H. Müller, J. Magn. Magn. Mater. **307**, 288 (2006).
 - ¹⁴ G. V. Pai, S. R. Hassan, H. R. Krishnamurthy, and T. V. Ramakrishnan, Europhys. Lett. **64**, 696 (2003).
 - ¹⁵ A. H. Morrish, B. J. Evans, J. A. Eaton, and L. K. Leung, Can. J. Phys. **47**, 2691 (1969).
 - ¹⁶ J. S. Kouvel and M. E. Fisher, Phys. Rev. **136**, A 1626 (1964).
 - ¹⁷ M. Dudka, R. Folk, Yu. Holovatch, and D. Ivaneiko, J. Magn. Magn. Mater. **256**, 243 (2003).
 - ¹⁸ M. Dudka, R. Folk, and Yu. Holovatch, J. Magn. Magn. Mater. **294**, 305 (2005).
 - ¹⁹ A. Möbius, C. Frenzel, R. Thielsch, R. Rosenbaum, C.J. Adkins, M. Schreiber, H.-D. Bauer, R. Grötzschel, V. Hoffmann, T. Krieg, N. Matz, H. Vinzelberg, and M. Witcomb, Phys. Rev. B **60**, 14209 (1999).
 - ²⁰ M. Camprostrini, M. Hasenbusch, A. Pelissetto, P. Rossi, and E. Vicari, Phys. Rev. B **65**, 144520 (2002).
 - ²¹ M. Sahana, U. K. Rössler, Nilotpal Ghosh, Suja Elizabeth, H. L. Bhat, K. Dörr, D. Eckert, M. Wolf, and K.-H. Müller, Phys. Rev. B **68**, 144408 (2003).
 - ²² Nilotpal Ghosh, Sahana Rössler, U. K. Rössler, K. Nenkov, Suja Elizabeth, H. L. Bhat, K. Dörr, and K.-H. Müller, J. Phys.: Condens. Matter **18**, 557 (2006).
 - ²³ Run-Wei Li, Xin Zhou, Bao-Gen Shen, and Burkhard

- Hillebrands, Phys. Rev. B **71**, 92407 (2005).
- ²⁴ R.B.Griffiths, Phys. Rev. Lett. **23**, 17 (1969).
- ²⁵ M.B. Salamon, P. Lin, and S.H. Chun, Phys. Rev. Lett. **88**, 197203 (2002); M.B. Salamon and S.H. Chun, Phys. Rev. **68**, 014411 (2003).
- ²⁶ J.Deisenhofer, D. Braak, H.-A. Krug von Nidda, J. Hemberger, R.M. Eremina, V.A. Ivanshin, A.M. Balbashov, G. Jug, A. Loidl, T. Kimura, and Y. Tokura, Phys. Rev. Lett. **95**, 257202 (2005).
- ²⁷ A. Weinbrib and B.I. Halperin, Phys. Rev. B **27**, 413 (1983).
- ²⁸ V.V. Prudnikov, P.V. Prudnikov, and A.A. Fedorenko, J. Phys. A: Math. Gen. **32**, 8587 (1999).
- ²⁹ V. Blavats'ka, C. von Ferber, and Yu. Holovatch, Phys. Rev. B **67**, 094404 (2003).
- ³⁰ S. Rössler, U. K. Rössler, K. Nenkov, D. Eckert, S.M. Yusuf, K. Dörr, and K.-H. Müller, Phys. Rev. B. **70**, 104417 (2004).
- ³¹ F. Rivadulla, J. Rivas, and J.B. Goodenough, Phys. Rev. B **70**, 172410 (2004).
- ³² A. Aharony and E.Pytte, Phys. Rev. Lett. **45**, 1583 (1980).
- ³³ P.M. Gehring, M.B. Salamon, A. del Moral, and J.I. Arnaudas, Phys. Rev. B **41**, 9134 (1990).
- ³⁴ A. Perumal, V. Srinivas, V.V.Rao, and R.A. Dunlap, Phys. Rev. Lett. **91**, 137202 (2003).